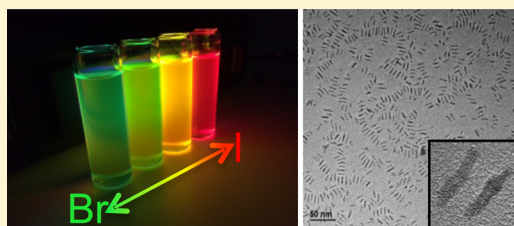# Two Dimensional Organometal Halide Perovskite Nanorods with Tunable Optical Properties

Sigalit Aharon and Lioz Etgar*

The Institute of Chemistry, Casali Center for Applied Chemistry, The Hebrew University of Jerusalem, Jerusalem, Israel

Ⓢ Supporting Information

ABSTRACT: Organo-metal halide perovskite is an efficient light harvester in photovoltaic solar cells. Organometal halide perovskite is used mainly in its "bulk" form in the solar cell. Confined perovskite nanostructures could be a promising candidate for efficient optoelectronic devices, taking advantage of the superior bulk properties of organo-metal halide perovskite, as well as the nanoscale properties. In this paper, we present facile low-temperature synthesis of two-dimensional (2D) lead halide perovskite nanorods (NRs). These NRs show a shift to higher energies in the absorbance and in the photoluminescence compared to the bulk material, which supports their 2D structure. X-ray diffraction (XRD) analysis of the NRs demonstrates their 2D nature combined with the tetragonal 3D perovskite structure. In addition, by alternating the halide composition, we were able to tune the optical properties of the NRs. Fast Fourier transform, and electron diffraction show the tetragonal structure of these NRs. By varying the ligands ratio (e.g., octylammonium to oleic acid) in the synthesis, we were able to provide the formation mechanism of these novel 2D perovskite NRs. The 2D perovskite NRs are promising candidates for a variety of optoelectronic applications, such as light-emitting diodes, lasing, solar cells, and sensors.

KEYWORDS: Perovskite, nanorods, absorption, photoluminescence, X-ray diffraction, transmission electron microscope

During the past several years, organometal halide perovskite (OMHP) has been demonstrated to be an efficient light harvester in solar cells. In some cases it functions simultaneously as absorber and as a hole conducting layer in the solar cell.[1−4] OMHPs can be used in several solar cell architectures, like mesoporous, planar, and without hole transporting layer.[5,3,6,7] To date, the highest certified power conversion efficiency of perovskite-based solar cells is 22.1%.[8]

The basic OMHP consists of corner sharing metal halide octahedra, in which a divalent metal cation satisfies the charge balance.[9,10] The dimensions of the final perovskite are dictated by the organic cation's size. Small organic cations, such as methylammonium (MA) or formamidinium, form the 3D perovskite structure, while large organic cations, such as ethylammonium, form the 2D perovskite structure.[11,12]

Confined perovskite nanoparticles could be utilized for the fabrication of highly efficient optoelectronic devices, taking advantage of their superior bulk properties as well as the nanoscale properties. Moreover, it has been reported that reducing the size of the OMHPs to the nanometric scale could enhance the photoluminescence (PL) emission.[1,13,14] Currently, there are several reports on the synthesis of perovskite quantum dots (QDs); most of them are related to the synthesis and characterization of all-inorganic perovskite QDs.[15−17] The synthetic technique of inorganic perovskite QDs is based on the ionic metathesis reaction, in which the kinetics of the nucleation and the growth are very fast. This route is not usable in the case of OMHP due to temperature and stability issues, as well as dissolving and precipitation problems. Because

of the temperature and the stability issues, which make the formation of standalone perovskite QDs/nanostructures challenging, a new synthetic route should be developed.

In a recent paper, Schmidt et al. reported the preparation of $MAPbBr_3$ nanoparticles (NPs) using (in combination with oleic acid) a medium sized alkyl-amine that controls the particles' growth and enables dispersing them in organic solvents. The $MAPbBr_3$ NPs demonstrated narrow emission with approximately 20% quantum yield (QY).[18] Zhu et al. synthesized $MAPbX_3$ (X = I− or Br−) NPs in several morphologies resulting in a mixture of dots, rods, wires, and sheets in the same sample. Generally, the synthetic process included the injection of several precursors into vigorously stirred toluene. In this method, besides the QDs (which were not stable and went through fast aggregation), all the synthesized morphologies had one or two nanometric dimension(s), while the third dimension was micrometric. Notably, the PL-QY of the various morphologies was very low.[19] Zhang et al. used a similar synthetic approach and synthesized highly luminescent $MAPbX_3$ QDs (X = I−, Br−, or Cl−). It was shown that by alternating the halides composition, different optical properties were achieved. The strong PL of the QDs originates from the increased exciton binding energy in combination with bromide-rich surface passivation.[20] Recently, Huang et al. showed that by using the injection method of several precursors into vigorously
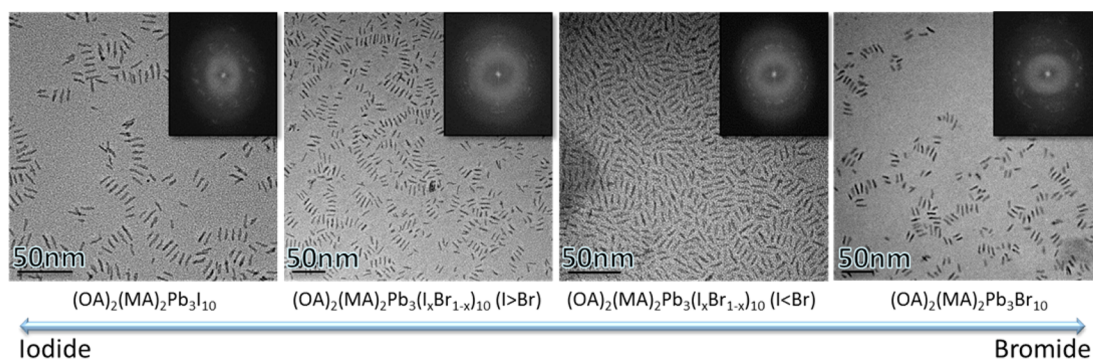
Figure 1. TEM images and inset FFTs of the NRs made of various halides compositions.

Table 1. Crystallographic Data of the Different NRs Compositions, Extracted from FFTs (see Figure 1 Inset)[a]

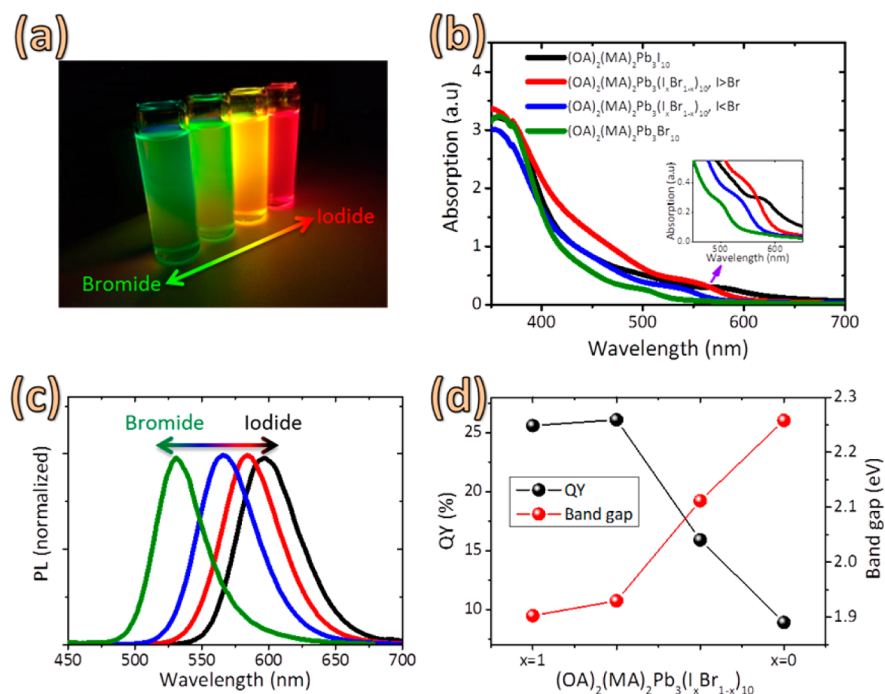| $(OA)_2(MA)_2Pb_3I_{10}$		$(OA)_2(MA)_2Pb_3(I_xBr_{1-x})_{10}$, I > Br		$(OA)_2(MA)_2Pb_3(I_xBr_{1-x})_{10}$, I < Br		$(OA)_2(MA)_2Pb_3Br_{10}$	
d-spacing (Å)	(hkl)	d-spacing (Å)	(hkl)	d-spacing (Å)	(hkl)	d-spacing (Å)	(hkl)
1.81	(404)	2.55	(312)	1.82	(404)	1.76	(226)
2.55	(312)	3.15	(004)	2.56	(312)	2.54	(312)
2.80	(310)	3.12	(220)	3.18	(004)	3.12	(220)
3.15	(004)					3.17	(004)

[a]$C_8H_{17}NH_3$ = OA, CH_3NH_3 = MA.

Figure 2. (a) Photo of the emitting NRs dispersions composed of various halides mixtures. (b) Absorbance spectra of the 2D perovskite NRs made of various halides compositions. (c) PL spectra of the 2D perovskite NRs made of various halides compositions. (d) PL-QY and band gap energies measured and calculated by Tauc plot of the perovskite NRs compositions.

stirred toluene the optical properties of MAPbBr₃ could be controlled by changing the precipitation temperature.[21] An additional synthetic method is the fabrication of OMHP QDs by emulsion, which assists in the size tuning of MAPbBr₃ QDs.[22]

This work describes facile low temperature synthesis of 2D perovskite nanorods in the structure $(C_8H_{17}NH_3)_2(CH_3NH_3)_2Pb_3(I_xBr_{1-x})_{10}$, $0 > x > 1$. The NRs were characterized by X-ray diffraction (XRD), electron diffraction (ED), and fast Fourier transform (FFT) analysis.

The XRD pattern reveals the 2D nature of the NRs combined with the 3D tetragonal perovskite structure. The absorbance and the PL of the NRs show a shift to higher energies compared with the bulk materials. In addition, changing the halide composition enables tunability of the NRs band gap. Various ligands ratios were studied and analyzed by high-resolution transmission electron microscopy (HR-TEM), which assisted in revealing the formation mechanism of these novel 2D perovskite NRs.

Figure 1 presents TEM images of the synthesized 2D perovskite NRs of the structure $R_2(MA)_{n-1}M_nX_{3n+1}$, where (R = OA = Octylammonium = $C_8H_{17}NH_3^+$; MA = methylammonium = $CH_3NH_3^+$; M = Pb^{2+}; X = I^- or Br^-, $0 < n < 3$).[23,24,26] The halide composition did not affect the NRs shape and size; the average size of the NRs is 2.25 ± 0.3 nm width and 11.36 ± 2.4 nm length. Larger TEM magnification of the various NRs compositions is shown in figure S1 in the Supporting Information (SI). The crystallographic structure of the NRs was analyzed using FFT as indicated at the inset of Figure 1. Table 1 shows the d-spacing values which were taken from the FFT analysis and the corresponding Miller indices for the various compositions. XRD and electron diffraction (ED) patterns of the 2D NRs were measured; the results are presented in Figure S2 and Table S1. The XRD characterization shows that the perovskite NRs have 2D perovskite structure combined with 3D tetragonal structure (described in more details below). It can be observed that the introduction of bromide ions into the perovskite structure changes the tetragonal lattice parameters from $a = b = 8.856$ Å, $c = 12.674$ Å for $(OA)_2(MA)_2Pb_3I_{10}$ to $a = b = 8.611$ Å, $c = 12.234$ Å for $(OA)_2(MA)_2Pb_3(I_xBr_{1-x})_{10}$ (I > Br), $a = b = 8.484$ Å, $c = 12.294$ Å for $(OA)_2(MA)_2Pb_3(I_xBr_{1-x})_{10}$ (I < Br) and $a = b = 8.474$ Å, $c = 11.943$ Å for pure $(OA)_2(MA)_2Pb_3Br_{10}$ as described previously for bulk perovskite[25] where the lattice parameter changes due to the smaller ionic radius of the Br^- compared with I^-.

Apart from the typical XRD pattern as an indication for the tetragonal perovskite structure, additional diffraction peaks are observed at angles below 14° (these peaks are also reported by Hassan et al. in the case of $n = 3$, see ref 24). The peaks below 14° are characteristic for 2D perovskite structure, and they are originated from the diffraction of the X-rays with the $(00n)$ facets of the 2D perovskite crystal ($n = 2, 4, 6...$) as indicated by Mitzi et al.[26] Using the angle at the (002) peak (the angles range between $5.3° - 6.5°$ depends on the I to Br concentration), we were able to calculate the d-spacing of the 002 plane ($d_{(002)}$) and the lattice parameter "c" of the resulting perovskite (for more details see the calculations in the SI). According to these calculations, the lattice parameter c of the various NRs composition is larger than the tetragonal c (as an example, for the pure-iodide sample, the $c_{tetragonal}$ is 12.674 Å while for the c_{2D} it is 27.19 Å, thus $c_{2D} \approx 2c_{tetragonal}$). This is an unambiguous evidence for the 2D nature of the NRs.

The optical characterizations of the 2D perovskite NRs are presented in Figure 2, including absorbance and PL; see Figure 2b,c, respectively. The absorbance spectra of the various compositions are not similar to the absorbance of the bulk perovskite with the same halide compositions; $MAPbI_3$ and $MAPbBr_3$ bulks absorb until ~800 and ~550 nm, respectively,[27] while the $(OA)_2(MA)_2Pb_3I_{10}$ NRs and $(OA)_2(MA)_2Pb_3Br_{10}$ NRs absorb only until ~650 and ~530 nm, respectively (Figure 2b).

The difference in the absorbance is attributed to two main contributions. The first is related to the use of octylammonium as ligand in the NRs synthesis. Octylammonium is larger than methylammonium, thus it cannot incorporate into the perovskite structure. The octylammonium is attached through its alkyl chain to the perovskite and limits the crystal growth in the attachment direction (additional details regarding the growth mechanism of these NRs are discussed below).[18] Because the perovskite growth is limited, the perovskite NRs are formed in a 2D perovskite structure that causes a shift in the absorbance and PL to shorter wavelength (higher energies) and hence to larger band gaps. Moreover the absorbance spectra observed in this work matches the reported absorbance of layered perovskite where $n = 3$.[28,23,24]

The second contribution is related to the halide exchange that includes the introduction of bromide ions into the $(OA)_2(MA)_2Pb_3I_{10}$ NRs (and the exclusion of iodide ions, respectively). The Br(4p) orbitals with the Pb(6s) orbitals determine the energy of the absorption peak, which is related to the valence band. It was shown that the transitions in PbI_2 are similar to the transitions in $MAPbI_xBr_{3-x}$ ($0 > x > 3$).[29,30] The conduction band of PbI_2 is composed of Pb(6p) orbitals, while its valence band composed of Pb(6s) orbitals and I(5p) orbitals. Further, the energy of the Br(4p) orbitals is lower than the energy of Pb(6s) orbitals; therefore, the absorption peak position of $(OA)_2(MA)_2Pb_3(I_xBr_{1-x})_{10}$, $0 > x > 1$ is influenced and shifted to higher energy (lower wavelength).[31] This shift can be observed in Figure 2b,c: an increase in the bromide concentration shifts the absorption and the PL to higher energies. Figure 2a presents the visual emission from the NRs in various compositions from iodide to bromide. It can be observed that the pure $(OA)_2(MA)_2Pb_3I_{10}$ has a red emission, which supports the PL and the absoption measurements.

Finally, in order to calculate the band gap energies (E_g) of these NRs, Tauc plots were plotted for the various samples. The Tauc plots are given in Figure S3, and the calculated E_g values are presented in Figure 2d (red). Like in the case of the bulk methylammonium lead halide perovskites, as the Br/I ratio increases the materials' E_g rises. Importantly, the 2D perovskite NRs E_g values are in the range of $1.9-2.26$ eV due to the dimensional changes.

The PL-QY of the various NRs compositions is presented in Figure 2d (black). The PL-QY is close to 30% for the $(OA)_2(MA)_2Pb_3I_{10}$ NRs and for the $(OA)_2(MA)_2Pb_3(I_xBr_{1-x})_{10}$ (I > Br) NRs. This PL-QY is relatively high compared to standard $MAPbI_3$ where PL-QY of close to 0% was measured. When the Br concentration is increased, the PL-QY is decreased. Feldmann et al.[32] have reported similar PL-QY for the perovskite nanostructures they studied. PL-QY of 20% was demonstrated for $MAPbBr_3$ nanoparticles which were synthesized in a medium of alkyl-amine that controls the particle growth,[19] and Hassan et al. measured 20% QY for 2D perovskite NPs.[24]

The main factor influencing the formation of the NRs is the organic moieties present in the synthesis. Three organic molecules were used in these syntheses: methylammonium iodide/bromide (MAI/MABr), octylammonium iodide (OAI), and oleic acid (OAc). The long chain of the octylammonium iodide cannot be incorporated into the perovskite crystal. Instead it attached to specific sites on the perovskite surface inhibiting the growth in a particular direction. In addition, the presence of OAc in the synthesis solution plays a role in the formation of the NRs as discussed below. To elucidate the formation mechanism of these 2D perovskite NRs, the ratio of OAc to OAI was studied. Different molar ratios of ligands (OAI and OAc) were studied while keeping all other conditions constant (see Experimental Section).

The OAI/OAc ratio which at the NRs that discussed in this paper are formed is OAI/OAc = 0.186. Therefore, ratios of 100% OAc, OAI/OAc = 0.075 (lower than the standard ratio), OAI/OAc = 0.250 (higher than the standard ratio) and 100% OAI were investigated.
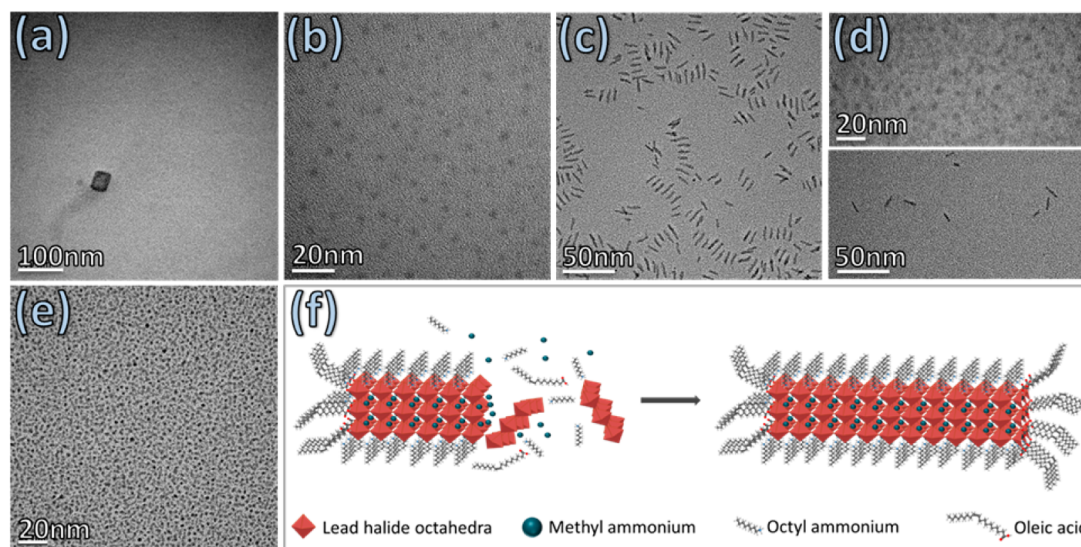
Figure 3. (a−f) TEM image of MAPbI₃ QDs/NRs that were prepared at various OAI/OAc ratios: (a) 100% OAc; (b) OAI/OAc = 0.075; (c) OAI/OAc = 0.186; and (d) OAI/OAc = 0.250 (the two figures are taken from the same sample in different areas); (e) 100% OAI. (f) Schematic illustration of the suggested NRs formation mechanism; the OAI and the OAc are presented schematically in the figure, whereas the blue dots represent the methylammonium and the red rhombus represent the PbI₂.

TEM images were recorded for the OAI/OAc ratios (Figure 3a−e). For 100% OAc (without OAI in the solution), there was no indication of the formation of nanostructures; the perovskite was formed as a bulk which precipitated at the bottom of the vial (Figure 3a shows empty TEM grid). For OAI/OAc= 0.075, the formation of QDs was observed, although their concentration was low (Figure 3b). When higher ratios were studied, for example, OAI/OAc = 0.250, both QDs and NRs were observed, indicated in Figure 3d; for 100% OAI, a high concentration of QDs was observed (Figure 3e).

These results indicate the difference in the adsorption affinity of the ligands to the NRs perovskite surface. At 100% OAc, no QDs were observed, which means that the OAc could not inhibit the perovskite growth. However, at 100% OAI, a high concentration of QDs was observed, suggesting that the OAI inhibits perovskite growth and attached strongly to the perovskite surface. The presence of iodide in the OAI assisted in the attachment of this alkyl chain to the QDs/NRs perovskite surface since it intercalates to the octahedral holes of the perovskite structure. This type of adsorption is called "chemisorption", because the interaction between the ligand and the surface lead to the formation of chemical interaction. On the other hand, the interaction of the OAc−perovskite interface is "physisorption", which means that the adsorption of the OAc upon the perovskite surface is physical and not as strong as the chemical interaction between the OAI−perovskite interface.

When varying the ratio to 0.250 (excess of OAI relative to the standard), QDs and NRs are formed, indicated by the two images in Figure 2d that were taken from the same sample. For a ratio of 0.075 (excess of OAc relative to the standard), the formation of NRs were rare. Therefore, it can be concluded that the OAI is attached to the NRs surface, while the OAc has an important role by shaping these QDs into NRs. As described above, the OAI attachment is much stronger to the NRs surface than that of the OAc because it fills the octahedral hole. The NRs are formed by the addition of monomers along specific axis, while the other axes are blocked by high affinity ligands absorbed to the surface (Figure 3f). The presence of the two

ligands is essential for the formation of the NRs. As discussed, the OAI has higher affinity to the perovskite surface than the OAc, so that for OAI/OAc = 0.075, there are not enough OAI ligands to allow the formation of NRs (and even the QDs formation is low). When the ratio was increased to OAI/OAc = 0.250 with an excess of OAI, some NRs were formed with a high concentration of QDs due to the stabilization of the QDs by the OAI but the low concentration of OAc results in the formation of few NRs. Therefore, pure NRs formation is achieved only when there is a balanced ratio of OAI/OAc = 0.186. On one hand, there is enough OAI to stabilize the NRs perovskite surface, and on the other hand there is enough OAc to balance the growth into NRs shape.

Conclusions. This work presents the synthesis and characterization of 2D perovskite NRs of the structure $(C_8H_{17}NH_3)_2(CH_3NH_3)_2Pb_3(I_xBr_{1-x})_{10}$, $0 > x > 1$. The NRs were synthesized by a facile low temperature synthesis. The perovskite NRs show strong PL with very good size distribution. Their bang gap energies can be tuned by halide exchange varying between 1.9−2.26 eV for iodide to bromide, respectively. The wider band gap observed for these NRs is related to the characteristics of their 2D structure due to the use of OAI in their synthesis. XRD, ED, and FFT provide evidence for the crystallographic structure of these NRs. By studying different ligand ratios (OAI/OAc) of the NRs, we were able to provide their formation mechanism. These 2D perovskite NRs have excellent potential to be used in variety of optoelectronic applications.

Experimental Section. *Precursor Synthesis.* OAI was synthesized by reacting 1 mL of octylamine (99%, Sigma) with 2 mL of hydroiodic acid (57 wt % in water, Aldrich) and 14 mL of distilled water in 100 mL round-bottom flask at 0 °C for 2 h while stirring. The precipitate was recovered by evaporating the solvents at 50 °C using a rotary evaporator. The white raw product was washed with diethyl ether. The washing step was repeated several times. After filtration, the solid was collected and dried at 60 °C in a vacuum oven for 24 h.

Methylammonium iodide/bromide (MAI/MABr) was synthesized by reacting 27.8 mL of methylamine (40% in

methanol, TCI) with 30 mL of hydroiodic acid (57 wt % in water, Aldrich) or 23.32 mL of hydrobromic acid (48 wt % in water, Aldrich) in a 250 mL round-bottom flask at 0 °C for 2 h while stirring. The precipitate was recovered by evaporating the solvents at 50 °C using a rotary evaporator. The white raw product was washed with diethyl ether. The washing step was repeated several times. After filtration, the solid was collected and dried at 60 °C in a vacuum oven for 24 h.

NRs synthesis. One molar $PbI_2/PbBr_2$ (99%, Aldrich) and 0.63 M MAI/MABr/MAI:MABr = 1:1 solutions in DMF (Aldrich) were prepared under nitrogen atmosphere. The solutions were heated on a hot plate at 83 °C until fully dissolved. Fifteen milligrams of OAI and 100 μL of oleic acid (technical grade, 90%, Aldrich) were mixed with 2 mL of octadecene (technical grade, 90%, Aldrich) in a small vial for an hour. Then 100 μL of the 0.63 M MAI/MABr/MAI:MABr = 1:1 solutions in DMF were added, followed by the addition of 50 μL of 1 M $PbI_2/PbBr_2$ solution. Finally, 5 mL of chloroform (biolab) were added. The vial was centrifuged at 3000 rpm for 1 min. Then the liquid phase was transformed into a clean vial and again centrifuged for 5 min at 6000 rpm. In the case of various ligand compositions, the syntheses includes the following ratios of OAI/OAc: 100% OAc, 0.075, 0.186, 0.250, and 100% OAI.

Characterization. TEM and ED observations were carried out using a Tecnai F20 G2 (FEI Company, U.S.A.). The samples were prepared as follows: 3 μL drop of the NRs dispersion was placed on a copper grid coated with amorphous carbon film, followed by evaporation of the solvent by a vacuum pump. FFT was done using the program "digital micrograph". Absorption spectra were recorded using Jasco V-670 spectrophotometer. Photoluminescence (PL) measurements were performed using L-shaped spectrophotometer (Edinburgh Instruments FL920). The samples were excited using at 400 nm. The emission was collected at 90° at the range of 450−800 nm. Photoluminescence quantum yields (PL-QY) were measured using Hamamatsu absolute PL-QY spectrometer C11347. Transmission (for the Tauc plots) spectra was measured using Varian Cary 5000 UV−vis-NIR spectrophotometer. X-ray powder diffraction measurements were performed in grazing incidence X-ray diffraction (GIXRD) mode on the D8 Advance Diffractometer (Bruker AXS, Karlsruhe, Germany) with a goniometer radius of 217.5 mm, a secondary graphite monochromator, 2° Soller slits, and a 0.2 mm receiving slit. XRD patterns within the range 5−60° 2θ were recorded at room temperature using CuKa radiation (l 1/4 1.5418°A) with the following measurement conditions: tube voltage of 40 kV, tube current of 40 mA, step-scan mode with a step size of 0.02° 2θ, and counting time of 1−3 s per step. The value of the grazing incidence angle was 2.5°.

■ ASSOCIATED CONTENT

Ⓢ Supporting Information

The Supporting Information is available free of charge on the ACS Publications website at DOI: 10.1021/acs.nano-lett.6b00665.

HR-TEM figures of the NRs, XRD spectra of the various compositions, *d*-spacing calculations and tauc plots. (PDF)

■ AUTHOR INFORMATION

Corresponding Author

*E-mail: lioz.etgar@mail.huji.ac.il.

Author Contributions

L.E. planned the experiments and wrote the manuscript. S.A. performed the experiments and was involved in the discussions.

Notes

The authors declare no competing financial interest.

■ REFERENCES

(1) Kojima, A.; Ikegami, M.; Teshima, K.; Miyasaka, T. *Chem. Lett.* **2012**, *41*, 397−399.

(2) Kim, H.-S.; Lee, C.-R.; Im, J.-H.; Lee, K.-B.; Moehl, T.; Marchioro, A.; Moon, S.-J.; Humphry-Baker, R.; Yum, J.-H.; Moser, J. E.; Graïzel, M.; Park, N.-G. *Sci. Rep.* **2012**, *2*, 591.

(3) Aharon, S.; Gamliel, S.; Cohen, B.-E.; Etgar, L. *Phys. Chem. Chem. Phys.* **2014**, *16*, 10512−10518.

(4) Lee, M. M.; Teuscher, J.; Miyasaka, T.; Murakami, T. N.; Snaith, H. J. *Science* **2012**, *338*, 643−647.

(5) Graetzel, M. *Nat. Mater.* **2014**, *13*, 838−842.

(6) Gamliel, S.; Dymshits, A.; Aharon, S.; Terkieltaub, E.; Etgar, L. *J. Phys. Chem. C* **2015**, *119*, 19722.

(7) Liu, D.; Yang, J.; Kelly, T. L. *J. Am. Chem. Soc.* **2014**, *136*, 17116−17122.

(8) The latest high efficiency was taken from NREL PV map at http://www.nrel.gov/ncpv/images/efficiency_chart.jpg.

(9) Mitzi, D. B. *Progress in Inorganic Chemistry*; John Wiley & Sons, Inc.: New York, 1999; Vol. *48*, p 1.

(10) Mitzi, D. B. *Inorg. Chem.* **2000**, *39*, 6107.

(11) Eperon, G. E.; Stranks, S. D.; Menelaou, C.; Johnston, M. B.; Herz, L. M.; Snaith, H. J. *Energy Environ. Sci.* **2014**, *7*, 982−988.

(12) Im, J. H.; Chung, J.; Kim, S. J.; Park, N. G. *Nanoscale Res. Lett.* **2012**, *7* (1), 353.

(13) D'Innocenzo, V.; SrimathKandada, A. R.; De Bastiani, M.; Gandini, M.; Petrozza, Y. *J. Am. Chem. Soc.* **2014**, *136*, 17730−17733.

(14) Noel, N. K.; Abate, A.; Stranks, S. D.; Parrott, E. S.; Burlakov, V. M.; Goriely, A.; Snaith, H. J. *ACS Nano* **2014**, *8*, 9815−9821.

(15) Protesescu, L.; Yakunin, S.; Bodnarchuk, M. I.; Krieg, F.; Caputo, R.; Hendon, C. H.; Yang, R. X.; Walsh, A.; Kovalenko, M. V. *Nano Lett.* **2015**, *15*, 3692−3696.

(16) Bekenstein, Y.; Koscher, B. A.; Eaton, S. W.; Yang, P.; Alivisatos, A. P. *J. Am. Chem. Soc.* **2015**, *137*, 16008−16011.

(17) Akkerman, Q. A.; Motti, S. G.; Kandada, A. R. S.; Mosconi, E.; D'Innocenzo, V.; Bertoni, G.; Marras, S.; Kamino, B. A.; Miranda, L.; De Angelis, F.; Petrozza, A.; Prato, M.; Manna, L. *J. Am. Chem. Soc.* **2015**, *138*, 1010.

(18) Schmidt, L. C.; Pertegas, A.; Gonzalez-Carrero, S.; Malinkiewicz, O.; Agouram, S.; Espallargas, G. M.; Bolink, H. J.; Galian, R. E.; Perez-Prieto, J. *J. Am. Chem. Soc.* **2014**, *136*, 850−853.

(19) Zhu, F.; Men, L.; Guo, Y.; Zhu, Q.; Bhattacharjee, U.; Goodwin, P. M.; Petrich, J. W.; Smith, E. A.; Vela, J. *ACS Nano* **2015**, *9*, 2948−2959.

(20) Zhang, F.; Zhong, H.; Chen, C.; Wu, X.; Hu, X.; Huang, H.; Han, J.; Zou, B.; Dong, Y. *ACS Nano* **2015**, *9*, 4533−4542.

(21) Huang, H.; Susha, A. S.; Kershaw, S. V.; Hung, T. F.; Rogach, A. L. *Advances Science* **2015**, *2*, 1500194.

(22) Huang, H.; Zhao, F.; Liu, L.; Zhang, F.; Wu, X.; Shi, L.; Zou, B.; Pei, Q.; Zhong, H. *ACS Appl. Mater. Interfaces* **2015**, *7*, 28128−28133.

(23) Wu, X.; Trinh, M. T.; Zhu, X. Y. *J. Phys. Chem. C* **2015**, *119*, 14714.

(24) Hassan, Y.; Song, Y.; Pensack, P. D.; Abde Lrahman, A. I.; Kobayashi, Y.; Winnik, M. A.; Scholes, G. D. *Adv. Mater.* **2016**, *28*, 566−573.

(25) Aharon, S.; Cohen, B.-E.; Etgar, L. *J. Phys. Chem. C* **2014**, *118*, 17160−17165.

(26) Liang, K.; Mitzi, D. B.; Prikas, M. T. *Chem. Mater.* **1998**, *10*, 403−411.

(27) Noh, J. H.; Im, S. H.; Heo, J. H.; Mandal, T. N.; Seok, S. I. *Nano Lett.* **2013**, *13*, 1764−1769.

(28) Dou, L.; Wong, A. B.; Yu, Y.; Lai, M.; Kornienko, N.; Eaton, S. W.; Fu, A.; Bischak, C. G.; Ma, J.; Ding, T.; Ginsberg, N. S.; Wang, L.-W.; Alivisatos, A. P.; Yang, P. *Science* **2015**, *349* (6255), 1518−1521.

(29) Kitazawa, N. *Mater. Sci. Eng., B* **1997**, *49*, 233−238.

(30) Ishihara, T.; Takahashi, J.; Goto, T. *Phys. Rev. B: Condens. Matter Mater. Phys.* **1990**, *42* (17), 11099.

(31) Ishihara, T. *J. Lumin.* **1994**, *60−61*, 269−274.

(32) Sichert, J. A.; Tong, Y.; Mutz, N.; Vollmer, M.; Fischer, S.; Milowska, K. Z.; Garcia Cortadella, R. G.; Nickel, B.; Cardenas-Daw, C.; Stolarczyk, J. K.; Urban, A. S.; Feldmann, J. *Nano Lett.* **2015**, *15*, 6521−6527.